

2 MJO and its relationship to ENSO

3 by

4 Youmin Tang¹ and Bin Yu²

5 ¹ Environmental Science and Engineering

6 University of Northern British Columbia, Prince George, BC, Canada

7 ² Climate Research Division, Environment Canada, Toronto, ON, Canada

8 Revised version for JGR-Atmosphere

9 December 19, 2007

¹Corresponding author: Youmin Tang, Email: ytang@unbc.ca

10 Abstract

11 In this study, we detected the spatial and temporal characteristics of Madden-Julian Os-
12 cillation (MJO) using zonal winds at the surface and outgoing long-wave radiation (OLR)
13 from the NCEP-NCAR (U.S. National Center of Environmental Prediction-National Cen-
14 ter for Atmospheric Research) reanalysis product from 1981-2003. The results show that
15 MJO activity, represented by these two variables, has large variances around 10° off the
16 equator and over the near-equatorial western Pacific.

17 One central issue addressed in this study is MJO-ENSO (El Niño and Southern Os-
18 cillation) relationship. It has been found that there exists a statistically significant rela-
19 tionship between MJO in spring-summer and ENSO in autumn-winter. The relationship
20 of MJO-ENSO is nonlinear in nature and has a decadal variation. A much stronger sta-
21 tistical relationship of MJO-ENSO was found in the 1990s as compared to that in the
22 1980s. These findings were further verified using ECMWF (European Center for Medium-
23 Range Weather Forecasts) reanalysis product. The potential mechanisms responsible for
24 MJO-ENSO relationship are also discussed.

25 **Key words:** MJO, ENSO, MJO-ENSO relationship.

1 Introduction

MJO is the dominant component of the intraseasonal (30-90 days) variability in the tropical atmosphere. It is typically characterized by eastward-traveling circulation cells moving along the equatorial plane, observed mainly over the Indian Ocean and the western Pacific Ocean. The MJO involves variations in a variety of fields such as wind, sea surface temperature (SST), cloudiness, rainfall, and OLR. Spectral analyses generally indicate a peak of their energy densities around 30 to 90-day period and a distinctive wave number one structure in the zonal direction.

MJO has significant impact on global weather and climate anomalies. The active phase of the MJO often provides the environment for high-impact weather events (e.g. tropical cyclones; monsoon precipitation anomalies). Observational and theoretical work has also shown that MJO may have a significant influence on ENSO, and may thus have important implications for climate prediction, especially for the prediction of ENSO (e.g., Lau et al., 1989; McPhaden et al. 2006; Hendon et al. 2007; Tang and Yu 2007). Therefore, it has been of great interest to investigate the connection of MJO-ENSO. It was argued that the MJO can impact ENSO as a stochastic forcing (SF) like westerly wind burst (WWB)², which often occurs over the western equatorial Pacific during the onset of some El Niño events such as 1982/1983 and 1997/1998 (Yu and Rienecker 1998; Harrison and Geise 1991). Indeed, the role of SF on ENSO cycle has been addressed during TOGA (Tropical Ocean-Global Atmosphere), especially since the late 1990s. Many studies show that the effects of realistic SF applied to a hybrid or an intermediate coupled model in a regime that would otherwise be periodic are sufficient to produce irregularity generally consistent with observed ENSO signals. (Blanke et al. 1997; Eckert and Latif 1997; Kleeman and Moore 1997; Moore and Kleeman 1999; Zavala-Garay et al 2005). It has also been observed that anomalous SF activity in the western Pacific often proceeds ENSO

²MJO is substantially different from WWB, and has a much larger spatial and temporal scales and much less occurrence frequency than WWB.

51 events and could trigger or modify ENSO events by downwelling Kelvin waves (Webster
52 and Palmer 1997; McPhaden 1999).

53 Previous observation and modeling studies generally indicated that MJO activity often
54 precedes El Niño, however the statistically significant relationship between them has not
55 been well identified (e.g., Slingo et al. 1999; Hendon et al. 1999; Kessler et al. 2001). One
56 central question here is whether the link between MJO and ENSO is random in nature,
57 thereby no statistically significant relationship existing, or nonlinear thus widely used
58 linear statistical techniques being invalid? Recently, McPhaden et al. (2006) and Hendon
59 et al. (2007) found that MJO-ENSO relationship has seasonal dependence. Further Tang
60 and Yu (2007) demonstrated that the relationship is nonlinear in nature. These studies
61 show significantly lagged correlations between MJO and ENSO indices.

62 In this study, we will further explore the relationship of MJO-ENSO using different
63 MJO indices, with emphases on its nonlinear, seasonal and decadal dependence. This
64 paper is structured as follows: Section 2 briefly describes the data and analysis techniques.
65 Section 3 detects the ENSO signals. Section 4 presents two estimates of MJO activity. In
66 section 5, we present a detailed analysis of MJO-ENSO relationship including its seasonal
67 dependence, decadal variation and nonlinearity, followed by conclusion and discussion in
68 section 6.

69 **2 Data and analysis techniques**

70 **2.1 Data**

71 The zonal winds at the surface and OLR were used to diagnose intraseasonal and MJO
72 activity. The data were obtained from daily NCEP-NCAR reanalysis product from Jan-
73 uary 1981 to December 2003 (<http://www.cdc.noaa.gov/cdc/data.ncep.reanalysis.html>).
74 We analyzed the data after 1979 considering that the introduction of satellite data in
75 1979 may bring some effects on the diagnosis. The NCEP-NCAR reanalysis product has

a various resolution for different variables with $2.5^\circ \times 2.5^\circ$ for zonal winds and $1.88^\circ \times 1.89^\circ$ for OLR. For further verification, we also used ERA-40 $2.0^\circ \times 2.0^\circ$ daily reanalysis zonal winds at the surface from 1981 to 2001 (Uppala et al. 2005). Observed SST is from Reynolds $2.0^\circ \times 2.0^\circ$ monthly dataset (Reynolds and Smith 1994). The SST is temporally interpolated to daily values using a linear scheme as in Zavala-Garay et al (2005). The climatology annual cycle for each calendar day is computed, and then subtracted from the raw data for each data set.

The domain of interest was spanned in the tropical Pacific from 15°S to 15°N , and 120°E to 70°W . We focus on the tropical Pacific ocean, since considerable evidences show that it is the MJO activity in the tropical Pacific, in particular in the western Pacific, that plays a critical role in influencing ENSO (e.g., Kessler 2001; McPhaden et al. 2006; Hendon et al. 2007; Tang and Yu 2007).

2.2 Analysis techniques

The empirical orthogonal function (EOF) is a widely used method to study a high-dimensional dataset in a low-dimensional space. It is capable of using few leading modes to describe dominant structures that explain the majority of overall variances. However EOF only depicts stationary modes that are unable to interpret propagation properties of the dataset, thus the time-lagged extended EOF (EEOF) analysis and Complex EOF (CEOF, e.g., Barnett, 1983) are employed in this study.

EEOF constitutes an extension of the traditional EOF technique to deal not only with spatial- but also with temporal correlations. It uses an extended matrix to compute covariance. The extended matrix is composed of a series of time-lagged data matrix, generated by the raw data matrix. Consider a space-time data matrix M with P spatial grids and N samples in time. Sliding a time window of length W over N ($W < N$) produces a time-lagged matrix. Moving the window forward and repeating the above process gets the second time-lagged matrix, and so forth. Therefore, the EEOF provides

not only eigenvectors but also the temporal evolutions of the eigenvectors. A detailed description of EEOF can be found in Tangang et al (1998).

CEOF analysis has been used in the past to detect wave propagating. Like EEOF, CEOF is another derivative of EOF. In CEOF, the covariance is computed using a complex matrix. The complex matrix \mathbf{U} should be constructed with the real data matrix \mathbf{M} using a Hilbert Transform, i.e., $\mathbf{U} = \mathbf{M} + \tilde{\mathbf{M}}$, where $\tilde{\mathbf{M}}$ is the imaginary part, generated by the Hilbert Transform as below,

$$\tilde{\mathbf{M}}(t) = \sum_{l=-L}^L \mathbf{M}(t-l)h(l) \quad (1)$$

where

$$h(l) = \begin{cases} \frac{2}{i\pi} \sin^2(l\pi/2) & \text{if } l \neq 0; \\ 0, & \text{if } l = 0. \end{cases}$$

Ideally $L = \infty$ in (1). In this study L is set to 7 as in Barnett (1983) and Zavala-Garay et al (2005).

Two important measures are often used in CEOF: amplitude function \mathbf{R} and phase function θ . The former represents the anomalous amplitude of an eigenvector whereas the latter depicts its propagation. Denote by \mathbf{B} an eigenvector, \mathbf{R} and θ are respectively defined as below

$$\mathbf{R} = \mathbf{B} * \mathbf{B}^*; \theta = \arctan\left[\frac{Im\mathbf{B}}{Re\mathbf{B}}\right] \quad (2)$$

where \mathbf{B}^* is conjugate of \mathbf{B} .

We also use two other statistical methods, singular value decomposition (SVD) and neural network (NN), to detect statistical relationship between variables. The former is a linear technique while the latter is nonlinear. In general, SVD captures optimally coupled spatial structures by maximizing the covariance between various possible patterns (Bretherton et al., 1992). The detailed formulation of the NN model is described in Tang et al. (2001).

3 ENSO signals

Since the ocean has a long-term memory in the coupled atmosphere-ocean system, the oceanic contribution is often the source of the low-frequency atmospheric variability. Based on Hasselmann’s hypothesis (1976), surface forcing can be decomposed into low-frequency slow components plus a residual, which primarily consists of random forcing representing fast atmospheric transients. As in Zavala-Garay et al (2005), we refer to the oceanic contribution as the ENSO-contribution and the residual as “non-ENSO” contribution.

We measure respectively the oceanic contribution to surface forcing by two statistical models, linear SVD and nonlinear NN. The season cycle was removed from datasets prior to performing SVD and NN analyses. It was found that the existing relationship between surface forcing and SST anomalies is essentially linear, and the nonlinear model shows little improvement. Thus we only present the results from the SVD method for simplicity in following.

Figs. 1a and 1b show the first singular vector for SST and zonal winds at the surface, accounting for 80.4% of total variance. In this mode, the warm (cold) water present in the equatorial eastern Pacific ocean corresponds with large westerly (easterly) wind anomalies over the equatorial central Pacific. This is a typical ENSO-like structure, suggesting a strong coupling between atmosphere and ocean in the equatorial and central Pacific ocean that can be described by the delayed oscillator theory (e.g., Tang and Hsieh, 2002).

Figs. 1c and 1d are the first singular vector for SST and OLR, accounting for 87.5% of total variance. The strong warming (cooling) in the eastern Pacific during El Niño (La Niña) leads to strong ascending (descending) motions where there is a large reduction (increase) in OLR, in association with a typically anomalous Walker circulation. At the region off the equator, the convergence (divergence) produces rise (subsidence) and cloudy (clear) sky conditions, also resulting in a decrease (increase) in OLR. Thus, a physical relationship between SST and tropical convection anomalies is clearly shown here.

149 To identify ENSO-like signal in surface forcing, we calculate the power spectrum at the
 150 ENSO frequencies. We define the total power at ENSO frequencies as the integral of the
 151 spectral density in the window with periods of 3-7 years as in Zavala-Garay et al. (2005).
 152 Fig. 2 shows respectively the power spectrum at ENSO frequencies for the raw zonal
 153 winds (Fig. 2a), for those estimated by the SVD model (Fig. 2b) and for the residual
 154 (Fig. 2c). ENSO signal is mainly present in the western-central equatorial Pacific in zonal
 155 winds. Comparing Fig. 2a and Fig. 2b reveals that the SST contribution from the SVD
 156 model explains most of ENSO signal. However there is still relatively weak ENSO signal
 157 in the residual field, probably excited by stochastically-induced Kelvin waves and Rossby
 158 waves. A similar picture emerges with OLR (not shown).

159 **4 MJO Signals**

160 Like the power definition for ENSO, we define the total power at MJO frequencies as the
 161 integral of the spectral density in the window with periods 30-90 days. Fig. 3 shows the
 162 power spectrum at MJO frequencies for zonal winds. The strong MJO signal appears in
 163 the off-equatorial region and in the western Pacific, whereas there is weak MJO signal
 164 in the central and eastern equatorial Pacific (Fig. 3a). The power structure for MJO is
 165 different from that for ENSO. In addition, A comparison between Fig. 3a and 3c reveals
 166 that the MJO signal is mainly contributed by atmospheric internal activities. The oceanic
 167 contribution (ENSO) to MJO is very weak (Fig. 3b). These features were also seen in
 168 the spectral analysis of the OLR (not shown).

169 The spatial and temporal characteristics of MJO can also be identified by employing
 170 a CEOF analysis. Shown in Fig. 4 is the spatial amplitude function of CEOF for zonal
 171 winds and OLR. A bandpass filter of 30-90 days⁻¹ was applied here prior to the CEOF
 172 analysis, so that only intraseasonal signals are kept in CEOF modes. The first CEOF
 173 modes explain 33% and 35% of total variance for zonal winds and OLR, respectively, both
 174 showing the strong MJO signal in the off-equatorial region of the western Pacific as noted

175 in Fig 3.

176 The strong MJO signal in the off-equatorial region as seen from Figs. 3 and 4 suggests
177 that the MJO activity represented by zonal winds at the surface and OLR is not spatially
178 symmetric about the equator. It should be noted that there are several other important
179 features for MJO, though some of them were directly diagnosed in this study: (1) MJO is
180 a 3-dimensional entity and has a varied representation by different variables. For example,
181 in boreal winter the maximum variance of MJO activity occurs in the equatorial eastern
182 Pacific in zonal winds at 200hPa but in around 10°S of the western Pacific in zonal winds at
183 850hPa and precipitation (Lin et al. 2007); (2) MJO has apparently seasonal variation,
184 characterized by a latitudinal migration across the equator between boreal winter and
185 summer (Zhang and Dong 2004). The seasonality in the MJO is pronounced in zonal
186 winds at the surface and low level (850hPa) and precipitation. Figs. 3 and Fig. 4 are
187 obtained in the sense of statistics, and do not preclude the possibility that MJO activity
188 has maximum variance over the equator at months such as spring or fall; (3) There is
189 always relatively large amplitude in the near-equatorial western Pacific in Figs. 3 and Fig.
190 4, which may excite down-welling Kelvin waves that propagate easterward and warm the
191 eastern Pacific. All these MJO features are important to help understand MJO-ENSO
192 connection as discussed in following sections.

193 Fig. 5 displays the recovered signal from the first CEOF mode, obtained by taking
194 the real part of the product of the first CEOF complex eigenvector multiplied by the
195 corresponding time series, for zonal winds and OLR, respectively. A short period from
196 1987-1991 was randomly chosen here for a clear presentation as in Zavala-Garay et al
197 (2005). Fig. 5 shows a pronounced MJO property, namely an apparent disturbance
198 propagating eastward from the western to the central and then the eastern Pacific Ocean.
199 In the following sections, we will use the first mode of CEOF to represent the MJO
200 activity as in some other studies (e.g., Zavala-Garay et al (2005); Tang and Yu (2007)).
201 In particular, we define the MJO index by the temporal amplitude function of the first

202 CEOF mode, which depicts the temporal evolution of the strength of MJO activity.

203 **5 MJO-ENSO relationship**

204 In this section, we will explore the MJO-ENSO relationship, with emphases on its non-
205 linear, seasonal and decadal dependence.

206 **5.1 Nonlinearity of MJO-ENSO relationship**

207 A conventional MJO index is usually defined as leading PCs (principal components) of
208 one or multiple fields (e.g., zonal winds or OLR). It has been shown that with such a kind
209 of MJO index, there is no statistically significant relationship between MJO and ENSO
210 (e.g., Slingo et al. 1999; Hendon et al. 1999; Kessler et al. 2001). On the other hand,
211 recently Hendon et al (2007) and McPhaden et al. (2006) found that the relationship of
212 MJO and ENSO varies with the season. Using the MJO index defined by the amplitude
213 of leading PCs of the combined fields of zonal winds at 850 hPa, 200 hPa and OLR, they
214 obtained significant correlation between boreal spring MJO activity and the subsequent
215 autumn/winter ENSO variability. Their work differs from previous studies in two as-
216 pects. The first is the MJO index itself. The amplitude function they used is essentially a
217 quadratic form of conventional PCs, therefore its linear correlation with ENSO could be
218 viewed as equivalent to a nonlinear relationship of a PC-defined MJO index onto ENSO.
219 The second is that they computed lagged correlation between MJO and ENSO indices
220 only using data of some seasons. It was found that the MJO-ENSO relationship is far
221 less significant when the data from all seasons were used (Hendon et al. 2007). Math-
222 ematically such a seasonal-dependent relationship could be described by a step function
223 (nonlinear), namely good linear relationship in some seasons and no linear relationship in
224 other seasons. Thus the overall relationship of MJO-ENSO is nonlinear in nature. This
225 might explain the reason why some of previous studies failed to identify significant rela-

226 tionship of MJO-ENSO when only linear components were considered. Indeed, the MJO
 227 and ENSO are dominant atmospheric and oceanic variability with different time scales,
 228 thus their relationship, if existed, is most likely nonlinear.

229 The evidence for the nonlinearity of MJO-ENSO relationship can be further demon-
 230 strated by correlating Nino3 index with conventional PC-defined MJO indices of zonal
 231 winds at the surface and OLR. The result shows that there is no significant correlation
 232 between the MJO and ENSO at all lags, even though the seasonal dependence is con-
 233 sidered as in Hendon et al. (2007)(not shown). This is consistent with earlier studies
 234 reported in Sligo et al. (1999) and Hendon et al. (1999).

235 Another work to examine the nonlinearity of MJO-ENSO relationship was documented
 236 in Tang and Yu (2007), where a nonlinear canonical correlation analysis (NLCCA) based
 237 on neural network was applied to PC-defined MJO index and ENSO index. With such
 238 a nonlinear statistical technique, a significant nonlinear correlation between MJO and
 239 ENSO can be identified, even though the seasonal dependence is not considered, namely
 240 samples of all seasons were used.

241 Therefore, a key issue in studying MJO-ENSO relationship is to consider its nonlin-
 242 earity, such as employing either data of some seasons (years) with conventional linear
 243 methods or data of all seasons (years) with nonlinear statistical methods. In this study,
 244 we will focus on the former. The time amplitude function of the first CEOF mode of zonal
 245 winds or OLR will be used as the MJO index, as discussed in section 4. We will refer to
 246 these amplitude time series, with daily sampling, as MJO_U or MJO_{OLR} . These indices
 247 are different from the index used in Hendon et al (2007) and McPhaden et al (2006)
 248 where a 90-day running mean was applied prior to computing correlation. That might
 249 bring concerns since a 90-day running mean could remove signal of the period under 90
 250 days.

5.2 Seasonal dependence of MJO-ENSO relationship

We first use all data samples to calculate lagged correlation between MJO and Nino3 indices. As expected, the correlation is very small for all lags from 0 to 240 days (not shown). As argued by Hendon et al (2007), the low correlation is the consequence of using all data samples. In fact, as we will see in following analyses, weak correlations in some seasons would greatly bias strong correlations in other seasons.

Shown in Fig. 6 is the lagged correlation function with lag time (abscissa) and start month (ordinate). The lag time is defined, unless otherwise indicated, by the time that MJO proceeds ENSO in this study. The lagged correlation was computed using the daily MJO index and the daily Niño3 (90°W to 150°W and 5°S to 5°N) SSTA index for the period from January 1, 1981 to December 31, 2003, and then averaged over calendar months. The correlation obtained by this means is almost identical to that computed using monthly data. Shaded in Fig. 6 are regions where the correlation is statistically significant at the confidence level of 95% by two-tailed student's t test ³.

Figs. 6a and 6b show both MJO_U and MJO_{OLR} in boreal summer significantly correlating with Niño3 SSTA several months later. Also MJO_{OLR} in boreal spring has a strong lagged relationship with Niño3 SSTA in the subsequent autumn-winter. Similar results were also obtained by Hendon et al. (2007), though they used a different MJO index.

Fig. 7 displays the correlation of MJO_U and MJO_{OLR} in July onto the tropical Pacific SSTA in the subsequent October. As can be seen, statistically significant correlation

³The number of degrees of freedom is estimated using the method introduced in Emery and Thomson (1998), namely,

$$N_{eff} = \frac{N}{\sum_{l=-L}^L [r_{xx}(l)r_{yy}(l) + r_{xy}(l)r_{yx}(l)]}$$

where $r_{..}(l)$ is the lagged correlation coefficient at a time lag of l , and x and y denote SSTA and MJO indices respectively. L is the maximum lag, set to $N/3$ here, and N is the original sample size. Unless otherwise indicated, the method is always used in following statistical tests.

regions cover the whole tropical eastern Pacific like an El Niño pattern (shaded area). In addition, the MJO_{OLR} produced more marked correlations with SSTA than MJO_U . Results from the correlations between MJO_{OLR} in May and SSTA in October show a similar feature (not shown).

The MJO activity is generally the strongest in boreal winter with the maximum variance occurring south of the equator in zonal winds at the surface and OLR, and a secondary maximum occurring north of the equator in boreal summer. The strong MJO activity near the equator tends to occur in boreal spring-early summer (Zhang and Dong 2004). One possible mechanism responsible for the connection of MJO-ENSO is through oceanic Kelvin waves. In an active MJO scenario, accompanying the eastward propagating MJO activity, large westerly wind anomalies bring warm water present in the central equatorial and eastern Pacific, which yields the warm SST and heat content (HC) anomalies in this region. A strong zonal HC gradient at the central equatorial Pacific weakens the upwelling there and intensifies the warm Kelvin waves propagating eastward. The warm eastward propagating Kelvin waves bring warm waters to the eastern Pacific ocean to further intensify the anomalies, leading to positive SST anomaly in the east. It has been found that there exists a significant relationship between the MJO-driven Kelvin waves and the strength of El Niño, with the Kelvin waves preceding El Niño by around 2-3 months (e.g., Zhang and Gottschalck 2002), which is very close to the time lag of maximum correlation between MJO activity in summer and subsequent El Niño in autumn-winter as shown in Fig. 6a.

While the above hypothesis explains the connection of MJO in summer with ENSO in autumn-winter, it might be unable to interpret the connection of MJO in spring with ENSO in autumn-winter as shown in Fig. 6b. This is because the lag time of the maximum correlation here is around 6 months, a time scale far larger than the time required for Kelvin waves across the Pacific basin. Another possible mechanism for MJO-ENSO relationship is based on Bjerknes theory of trade wind, first proposed by Bjerknes (1969)

and recently addressed by some researchers (e.g., Hendon et al. 2007; Kessler and Kleeman 2000). The core component here is the interaction between MJO-induced westerly anomalies with SST anomalies. It has been found that enhanced MJO activity often results in anomalous westerly surface winds in the western Pacific (e.g., Kessler and Kleeman 2000; Zavala-Garay et al. 2005). In general, the westerly anomalies in the western Pacific precede the development of El Niño through bringing surface warm water into the central and eastern Pacific. This process often starts in Spring. The warm water in the central and eastern Pacific enhances the SST zonal gradient there, and in turn intensifies westerly anomalies. Such a positive feedback between the westerly anomalies and SSTA in the central and eastern Pacific promotes enhanced MJO activity in the western Pacific, which then promotes enhanced surface westerlies in the western Pacific. These are highly conducive to El Niño conditions 6-8 months later as evidenced and argued in Hendon et al. (2007).

5.3 Decadal dependence of MJO-ENSO relationship

A clear contrast in terms of the characteristics of the interannual variability exists between the 1980s and the 1990s in the Pacific ocean, evidenced by many observations such as sea level pressure, SST, low-level zonal wind, and subsurface ocean heat content anomalies (e.g., Kleeman et al. 1996; Tang and Hsieh 2003). It is of interest to explore the impact of decadal variation of the interannual variability on MJO-ENSO relationship. Shown in Fig. 8 are lagged correlations calculated using the data during 1981-1990 and 1991-2000 respectively. The lagged correlations between MJO and ENSO as noted in section 5.2 are more pronounced in the 1990s as compared to that in the 1980s, especially for MJO_U . Such a decadal variation of MJO-ENSO relationship can be further demonstrated in Fig. 9, showing the correlation between MJO in May and the tropical SSTA in the subsequent October. As can be seen, the correlation displays an ENSO-like pattern for both decades with relatively large values occurring in the tropical eastern Pacific ocean, whereas the

325 correlation is less pronounced in the 1980s but more marked in the 1990s.

326 To examine the impact of finite sample size on correlation coefficients in Fig. 8 and
327 Fig. 9, we calculated the correlation between MJO in March-May and the tropical SSTA
328 in the subsequent October-December as shown in Fig. 10. As such, the sample size is
329 three times as much as that used in Fig. 9⁴. Fig. 10 is very similar to Fig. 9, further
330 suggesting that the impact of MJO on ENSO is weaker in the 1980s than in the 1990s.

331 Fig. 11 shows the MJO-ENSO correlations in the 1980s and 1990s, calculated using
332 data of all seasons. A striking decadal variation is clearly seen for both MJO_U and
333 MJO_{OLR} indices. Statistical tests indicate that the MJO-ENSO correlation is significant
334 at lags of 2-6 months for the 1990s at the 95% confidence level, but not significant at all
335 lags for the 1980s. Fig. 12 further compares MJO and ENSO indices for the period from
336 1981-2000. As expected, relatively strong MJO signal could be seen prior to several EL
337 Niño events. Such a lagged relationship is more visible in the 1990s. For example, the
338 MJO activity was strong before 1997 El Niño, but weak or absent prior to 1982 warm
339 event. On the other hand, there were more 'false alarms' in the 1980s, namely strong
340 MJO activities do not lead to EL Niño events.

341 It should be noticed that the decadal variation of MJO-ENSO relationship is not de-
342 pendent on the MJO indices used in this study. To address this, we repeated the above
343 analyses but used BMRC (Bureau of Meteorology of Research Center, Australia) MJO in-
344 dex (<http://www.bom.gov.au/bmrc/clfor/cfstaff/matw/maproom/index.html>), which was
345 developed by Wheeler and Hendon (2004) and has been used in many MJO studies (e.
346 g., McPhaden et al 2006; Hendon et al. 2007). Significant differences of MJO-ENSO
347 relationship between the 1980s and 1990s are also striking as shown in Figs. 13 and 14.
348 In addition, compared with Fig. 8a, Fig. 13a also shows some marginally significant
349 MJO-ENSO correlations in the 1980s, though far less pronounced compared with the

⁴However it does not mean the effective number of degree of freedom increases three times due to serial correlation existing in ENSO index. Instead, the effective number of degree of freedom increases from 10 to 21

350 correlation in the 1990s.

351 The decadal variation of MJO-ENSO relationship is probably associated with the vari-
352 ation of both atmospheric anomalies (such as MJO wind anomalies) and ocean anomalies
353 (SSTA) in the two decades. Shown in Fig. 15 are the first EEOF modes of zonal winds,
354 derived using the data of 1980s and 1990s respectively. Comparing the structure of EEOF
355 modes between the two decades reveals that MJO has a period of around 50 days in the
356 1990s and 60 days in the 1980s, associated with a faster eastward shift of MJO activity
357 and relatively stronger westerlies in the 1990s. The power spectrum analysis for the time
358 series of EEOF confirms a shorter period in the 1990s. As discussed in the above section,
359 the impact of MJO on ENSO is most likely through the low-frequency westerly anomalies
360 associated with enhanced MJO activity, which project efficiently onto the El Niño mode
361 in spring (Hendon et al. 2007). Indeed, the observations show that the westerly wind is
362 more prevailed over the equatorial western Pacific in the 1990s than in the 1980s (Tang
363 and Hsieh 2002). The westerly anomalies over the equatorial western Pacific bring warm
364 water to the central and the eastern Pacific, leading to El Niño conditions by either the
365 downing Kelvin waves or the SST-westerly wind positive feedback as discussed above.

366 5.4 Further verification of MJO-ENSO relationship

367 Based on the defined MJO indices, we have found significantly lagged correlations between
368 MJO and ENSO. The MJO-ENSO relationship displays both seasonal and decadal de-
369 pendence. These results were further confirmed using the BMRC MJO index. However it
370 is noted that the BMRC MJO index was also derived from NCEP-NCAR reanalysis prod-
371 uct. In this subsection, the MJO-ENSO relationship is further examined using ECMWF
372 ERA-40 reanalysis product.

373 We repeated all analyses performed in subsections 5.2 and 5.3 but used ECMWF
374 ERA-40 to derive the MJO index. Similarly, the MJO index was defined by the amplitude
375 function of the first CEOF. Correlating the ERA-40 MJO index with the tropical Pacific

376 SSTA shows that the MJO-ENSO relationship reported above can also be obtained using
 377 the ERA-40 MJO index. Fig. 16 is the lagged correlation of the ERA-40 MJO index
 378 with respect to the observed Niño3 SSTA index, as a function of lagged time and start
 379 month. Figs. 16a-c, highly resembling Fig. 6a, Fig. 8a and Fig. 8c, further verify
 380 the significant MJO-ENSO relationship obtained in proceeding sections. In addition, the
 381 lagged correlations of the ERA-40 MJO index in March-May onto the tropical SSTA in
 382 the subsequent October-December, as presented in Fig. 17 for both the 1980s and the
 383 1990s, also closely resemble Fig. 10 obtained using the NCEP-NCAR reanalysis product.
 384 These indicate that the MJO-ENSO relationship identified in this study is not dependent
 385 on reanalysis products, though it is worth noting that the ECMWF and NCEP-NCAR
 386 reanalysis products are related each other somehow due to the same real observations
 387 used in their data assimilations.

388 **6 Summary and Conclusion**

389 In this study, first, we analyzed the spatial and temporal characteristics of MJO using daily
 390 zonal winds at the surface and OLR of NCEP-NCAR reanalysis product for the period
 391 from 1981-2003. Two estimates were made to detect MJO signals. The first estimate is
 392 based on the intraseasonally passed timeseries. In the second estimate, we removed the
 393 contribution of ENSO to MJO with aid of an empirical model. The two estimates show
 394 very similar features in terms of both MJO spatial structure and temporal variability. The
 395 ENSO contribution to MJO is subtle whereas MJO activity, represented in the two fields,
 396 mainly exists around 10° off the equator and over the near-equatorial western Pacific.

397 We then focus on analyzing the MJO-ENSO relationship, the central issue addressed
 398 in this study. It has been found that there exists a significant relationship between MJO
 399 in spring-summer and ENSO in autumn-winter. Two possible mechanisms are responsible
 400 for this relationship. The relationship between MJO in summer and ENSO in autumn is
 401 probably related to the oceanic downwelling Kelvin waves, which are excited by eastward

402 propagating MJO activity in the equatorial western Pacific. The eastward propagating
 403 Kelvin waves bring warm water present in the tropical central and eastern Pacific, which
 404 yields the warm SST anomalies. For the relationship between MJO in spring and ENSO
 405 in autumn-winter, a positive feedback between MJO-induced westerly anomalies and the
 406 SST anomalies appears to be a major pathway. The anomalous westerly surface winds
 407 in the western Pacific associated with enhanced MJO activity bring surface warm water
 408 into the tropical central and eastern Pacific. The warm water enhances the SST zonal
 409 gradient there, and in turn intensifies westerly anomalies. The relationship between MJO
 410 in spring and ENSO in autumn-winter has also been addressed in Hendon et al. (2007).

411 One new finding in this study is that MJO-ENSO relationship has decadal variation.
 412 The relationship between MJO in spring-summer and ENSO in autumn-winter is much
 413 more significant in the 1990s than in the 1980s. This is most probably due to the decadal
 414 variation of MJO activity and ENSO variability. It has been found that during the 1990s,
 415 the MJO activity appeared more frequent, and the westerly wind was more prevailed
 416 over the equatorial western Pacific. As discussed in Hendon et al. (2007), the impact of
 417 MJO on ENSO is most probably through the low-frequency westerly anomalies that are
 418 associated with enhanced MJO activity and project efficiently onto the El Niño mode in
 419 spring. The strong westerly winds drive warm water to the tropical central and eastern
 420 Pacific to strengthen the development of El Niño.

421 Some cautions should be taken regarding the decadal variation of MJO-ENSO rela-
 422 tionship reported here. First, the finite effective samples used for the analysis is a concern.
 423 There are only four and five ENSO events in the 1980s and the 1990s respectively. The
 424 correlation coefficient obtained using daily data has a sample size of around 300 in Figs.
 425 8 and 9 and 900 in Fig. 10, however the effective number of degree of freedom is not as
 426 large due to the strong serial correlation in SST data. This might have an effect on the
 427 robustness of our results though statistical significance tests based on the effective num-
 428 ber of degree of freedom was performed. Second the data itself might have a contribution

429 to the decadal variation of MJO-ENSO relationship. During TOGA decade starting in
 430 1985 many new oceanic observational systems were gradually put in place which would
 431 have added more accuracy to the reanalyzed surface winds in NCEP-NCAR and ER40
 432 products. McPhaden et al (2006) also found a better relationship between MJO and
 433 ENSO indices after 1995 when the TAO array observational system was completed and
 434 provided oceanic upper thermal field data. On the other hand, the significant difference
 435 of MJO-ENSO relationship also exists between the 1980s and the 1990s in OLR. It was
 436 believed that the additional surface data would probably have little impact on the OLR.
 437 Nevertheless, the present analysis is to date the first exploratory work to discuss possi-
 438 ble decadal variation of MJO-ENSO relationship, which provides some insights into the
 439 impact of MJO on ENSO.

440 This study is also able to shed some lights on ENSO mechanisms. Nonlinear dynamics
 441 and stochastically forcing linear dynamics are two most widely accepted candidates for
 442 ENSO mechanisms. Indeed, the role of stochastically forcing on ENSO cycle has been
 443 addressed at various times, especially since the late 1990s. A key issue in studying the
 444 impact of stochastic forcing on ENSO is to extract large-scale stochastic forcing patterns
 445 responsible for ENSO behavior. This can be implemented by a linear stochastic dynamical
 446 framework introduced by Kleeman and Moore (1997), i.e., stochastic optimal of coupled
 447 models. Many studies have shown that the stochastic optimal of a coupled model is the
 448 forcing pattern most favored to trigger ENSO-like oscillation (e.g., Moore et al. 2006).
 449 Since MJO is a dominant atmospheric intraseasonal mode and has a large spatial and
 450 temporal scale, one may be able to use MJO to represent the stochastic optimal to study
 451 the response of ENSO to stochastic forcing. However, results from the present study
 452 also indicate that ENSO variability does not always rely on MJO forcing such as 1982
 453 El Niño event where the MJO forcing was absent. A more detailed investigation requires
 454 sensitivity experiments of the response of ENSO to MJO, which is under the way.

455 **Acknowledgments**

456 This work was supported by Canadian Foundation for Climate and Atmospheric Sciences
457 through its network of Global Ocean-Atmosphere Prediction and Predictability (GOAPP)
458 and Canada Research Chair program. We thank three anonymous reviewers for their
459 comments on the improvements of this paper.

References

- Barnett, T. P., 1983: Interaction of the Monsoon and Pacific Trade Wind System at Interannual Time Scales Part I: The Equatorial Zone. *Mon. Wea. Rev.*, **111**, 756-773.
- Bjerknes, J. P., 1969: Atmospheric teleconnections from the equatorial Pacific, *Mon. Wea. Rev.*, **97**, 163-172.
- Blanke, B., J. D. Neelin and D. Gutzler, 1997: Estimating the effect of stochastic wind stress forcing on ENSO irregularity. *J Climate*, **10**, 1473-1486.
- Bretherton, C. S., C. Smith, and J. M. Wallace, 1992: An Intercomparison of Methods for Finding Coupled Patterns in Climate Data. *J. Clim.*, **5**, 541-560.
- Eckert, C. and M. Latif, 1997: Predictability of a stochastic forced hybrid coupled model of El Niño. *J Climate*, **10**, 1488-1504
- Emery, W. J. and Thomson, R. E., 1998: Data Analysis Methods in Physical Oceanography, Pergamon, Elsevier Science, 400pp.
- Harrison, E.D, and Geise, B. S., 1991: Episodes of surface westerly winds as observed from islands in the western tropical Pacific. *J. Geophys. Res.*, **96**, 3221-3237.
- Hasselmann, K. F., 1976: Stochastic climate models. Part I. Theory. *Tellus*, **28**, 473-484.
- Hendon, H. H., C. Zhang, and J. Glick, 1999: Interannual variation of the Madden-Julian oscillation during austral summer. *J. Clim.*, **12**, 2538-2550
- Hendon, H. H., M. Wheeler, and C. Zhang, 2007: Seasonal dependence of the MJO-ENSO Relationship. *J. Climate*, **20**, 531-543.
- Kessler W., 2001: EOF Representations of the Madden-Julian Oscillation and its connection with ENSO, *J. Clim.*, **14**, 3055-3061.

- 483 Kessler, W. S., and R. Kleeman, 2000: Rectification of the Madden-Julian Oscillation
484 into the ENSO cycle *J. Clim.*, **13**, 3560-3575.
- 485 Kleeman, R., R. Colman, N. R. Smith and S. B. Power, 1996: A recent change in the
486 mean state of the Pacific ocean, Observational evidence, atmospheric and oceanic
487 responses. *J. Geophys. Res. (Oceans)*, **101**, 20483-20499.
- 488 — and A. M. Moore, 1997: A theory for the limitation of ENSO predictability due to
489 stochastic atmospheric transients, *J. Atmos. Sci.*, **54**, 753-767.
- 490 Lin, H., G. Brunet and J. Derome, 2007: Forecast skill of the Madden-Julian Oscillation
491 in two Canadian atmospheric models. *Mon. Wea. Rev.*, submitted.
- 492 Lau, K.M., L. Peng, T. Nakazawa, and C.H. Sui, 1989: Dynamics of super cloud clusters,
493 westerly wind bursts, 30-60 day oscillations and ENSO - An unified view. *J. Meteor.*
494 *Soc. Japan*, **67**, 205-219.
- 495 McPhaden J. M., 1999: Genesis and evolution of the 1997-98 El Nino. *Science*, **283**,
496 950-954.
- 497 McPhaden, J. M., X. Zhang, H. Henden and C. Wheeler, 2006: Large scale dynamics and
498 MJO forcing of ENSO variability. *Geophys. Res. Lett.*, **33**, L16702, doi:10.1029/2006GL026786.
- 499 Moore, A. and R. Kleeman, 1999: Stochastic forcing of ENSO by the Intraseasonal Os-
500 cillation. *J. Climate*, **12**, 1199-1220.
- 501 Moore, A. M., J. Zavala-Garay, Y. Tang, R. Kleeman, A. T. Weaver, J. Vialard, K.
502 Sahami and D. L. T. Anderson, 2006: Optimal Forcing Patterns for Coupled Models
503 of ENSO *J. Climate*, **19**, 4683-4699.
- 504 Reynolds, R. W. and T. M. Smith, 1994: Improved global sea surface temperature analysis
505 using optimal interpolation. *J. Clim.*, **7**, 929-948.

506 Slingo, J. M., D. B. Rowell, K. R. Sperber and F. Nortley, 1999: On the predictability
507 of the inner annual behavior of the Madden-Julian Oscillation and its relationship
508 with El Niño, *Quart. J. Roy. Met. Soc.*, **125**, 583-609.

509 Tang, Y and Hsieh, W. W, Tang, B and Haines, K, 2001: A neural network atmospheric
510 model for hybrid coupled modeling, *Climate Dynamics*, **17**, 445-455.

511 Tang, Y. and W.W. Hsieh, 2002. Hybrid coupled models of the tropical Pacific – ENSO
512 prediction. *Climate Dynamics*, **19**, 343-353.

513 Tang, Y. and B. Yu 2007: An analysis of nonlinear relationship between the MJO and
514 ENSO, *J. Geophys. Res.(Ocean)*, (submitted).

515 Tangang, F. T., B. Tang, A. H. Monahan, and W. W. Hsieh, 1998: Forecasting ENSO
516 Events: A Neural Network-Extended EOF approach, *J. Climate*, **11**, 29-41.

517 Uppala, S.M., et al., 2005: The ERA-40 reanalysis. *Q.J.R.Meteor.Soc.*, **131**, 2961-3012.

518 Webster, P. J. and T. N. Palmer, 1997: The past and future of El Nino. *Nature*, 390(12),
519 562-564.

520 Wheeler, M. C., and H. H. Hendon, 2004: An all-season real-time multivariate MJO
521 Index: Development of an index for monitoring and prediction. *Mon. Wea. Rev.*,
522 **132**, 1917-1932.

523 Yu, L., and M. Rienecker, 1998: Evidence of an extratropical atmospheric influence during
524 the onset of the 1997-98 El Nino. *Geophys. Res. Lett.*, **25**(18), 3537-3540.

525 Zavala-Garay J, C. Zhang, A. Moore, and R. Kleeman, 2005: On the linear response of
526 ENSO to the Madden Julian Oscillation, *J. Clim.*, , 2441-2459.

527 Zhang, C., and J. Gottschalck, 2002: SST anomalies of ENSO and the Madden-Julian
528 Oscillation in the equatorial Pacific. *J. Clim.*, **15**, 2429-2445.

529 —, and M. Dong, 2004: Seasonality of the Madden-Julian Oscillation. *J. Climate*, **17**,
530 3169-3180.

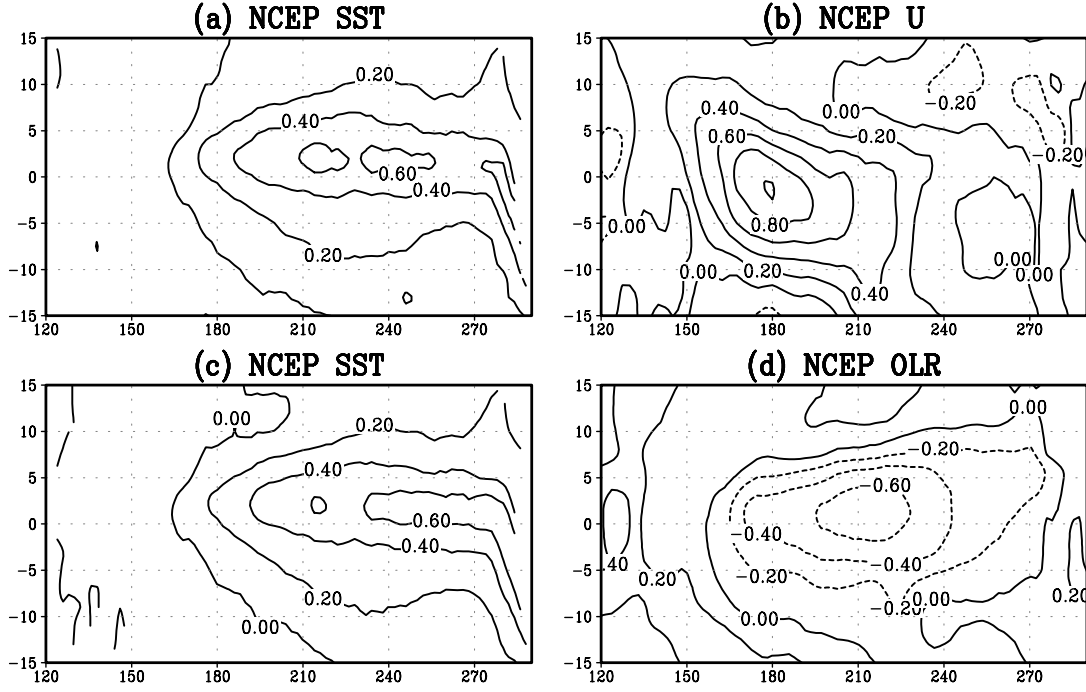


Figure 1: The leading SVD mode for SST-zonal winds (a and b), and for SST-OLR (c and d). The first modes account for 80.4% and 87.5% of total variance respectively. Unit is ms^{-1} for zonal wind, $^{\circ}C$ for SST and W/m^2 for OLR. The contour interval is 0.2.

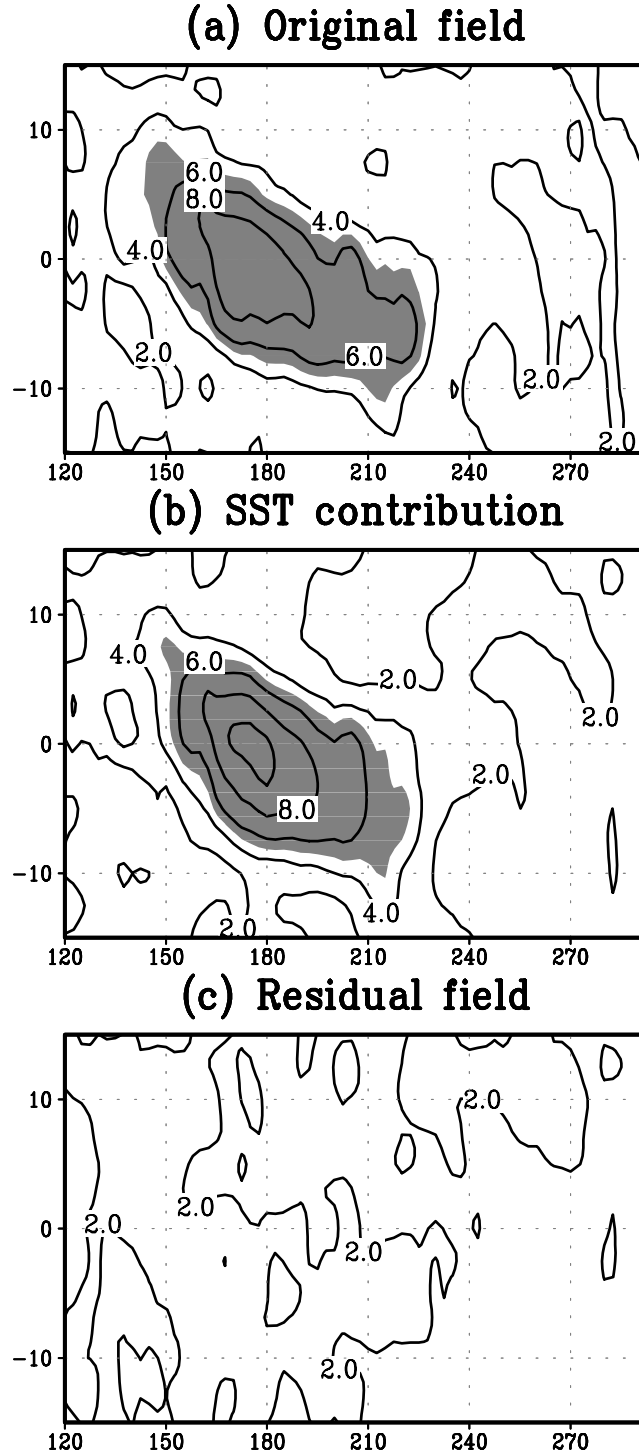


Figure 2: The spectrum power of ENSO frequency of 3-7 years in the NCEP reanalysis for zonal winds at the surface, (a) original winds; (b) estimated winds by the statistical model; (c) residual field between original and estimated winds. The unit is $m^2 s^{-2}$. Shaded are regions where the power has magnitude greater than 4, which was arbitrarily chosen for a good presentation. The contour interval is 2.

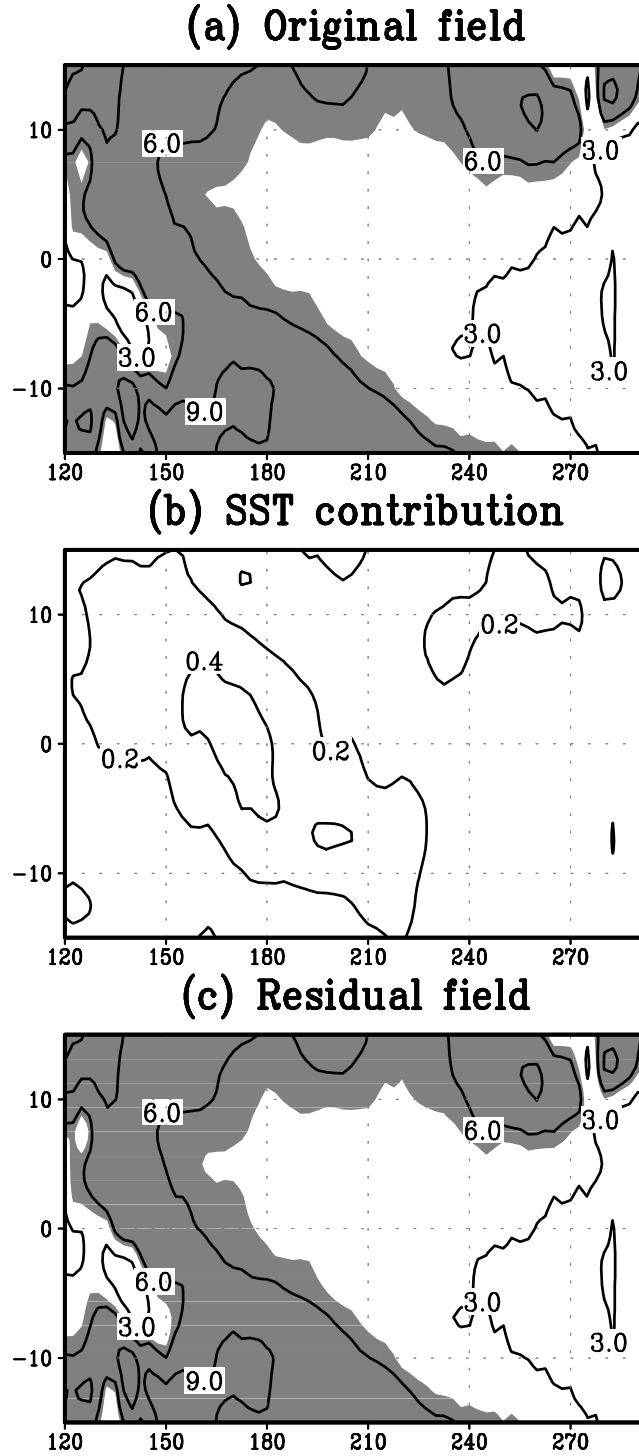


Figure 3: The spectrum power of MJO frequencies of 30-90 days for zonal winds (a) original winds; (b) estimated winds by statistical model; (c) residual field between original and estimated winds. The unit is $m^2 s^{-2}$. The magnitude of the power over 5 is shaded. The interval level is 0.2 for (b) and 3 for others.

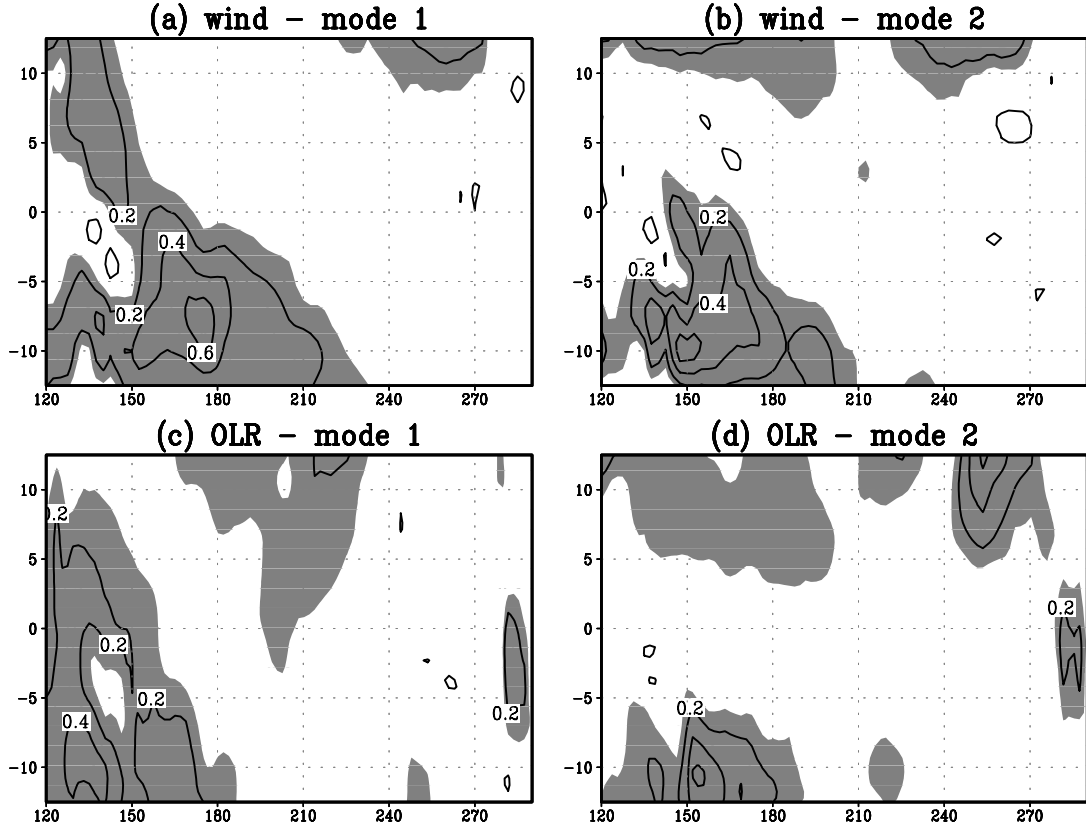


Figure 4: The first two leading CEOF spatial amplitude modes for zonal winds (a and b) and OLR (c and d). Shaded are regions where the value is over 0.1. The unit is m^2s^{-2} for zonal wind and W/m^2 for OLR. The contour interval is 0.2.

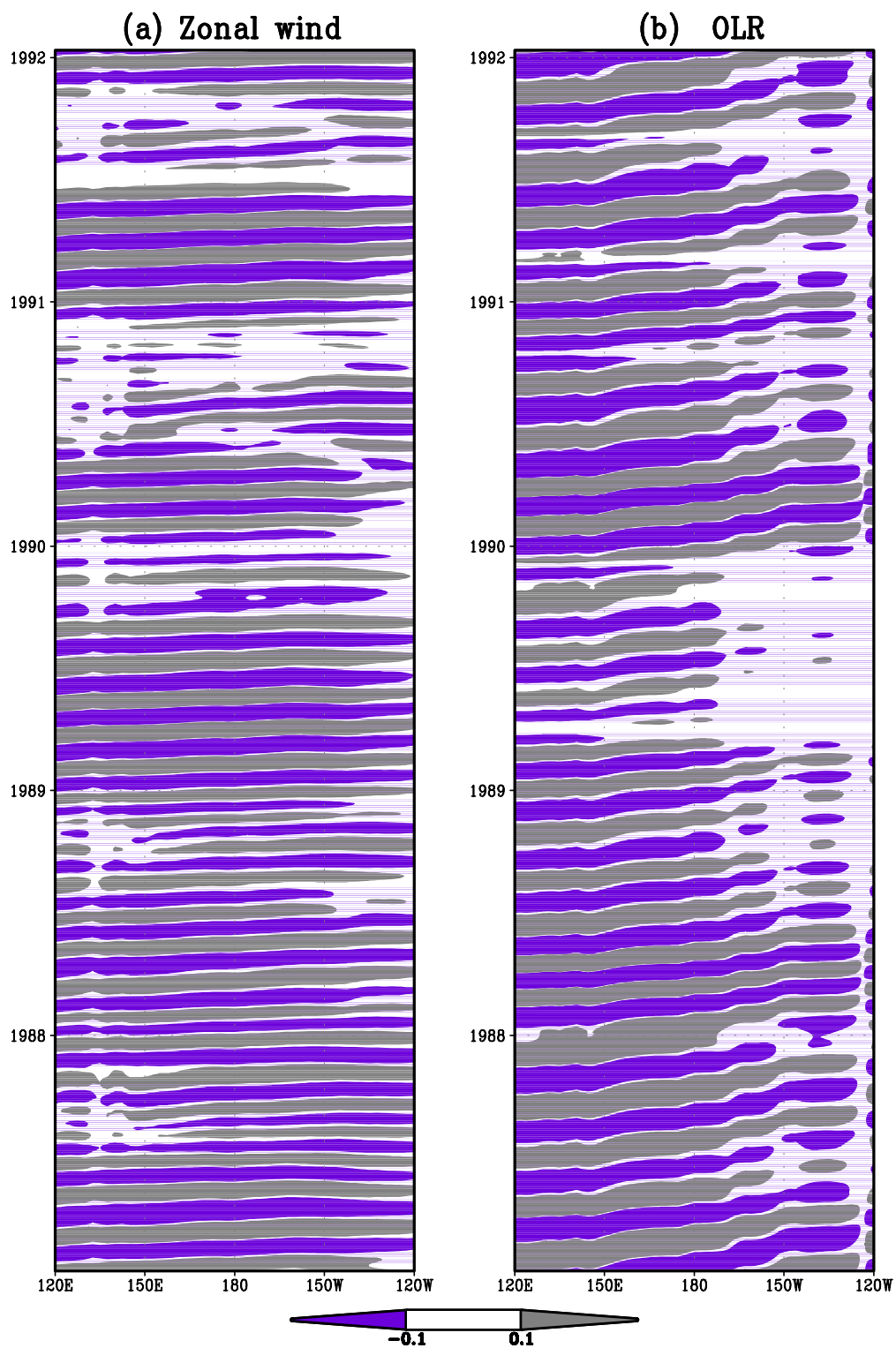


Figure 5: Time-longitude section of the recovered MJO signal using the first CEOF mode
²⁸
along 10°S for (a) zonal winds and (b) OLR.

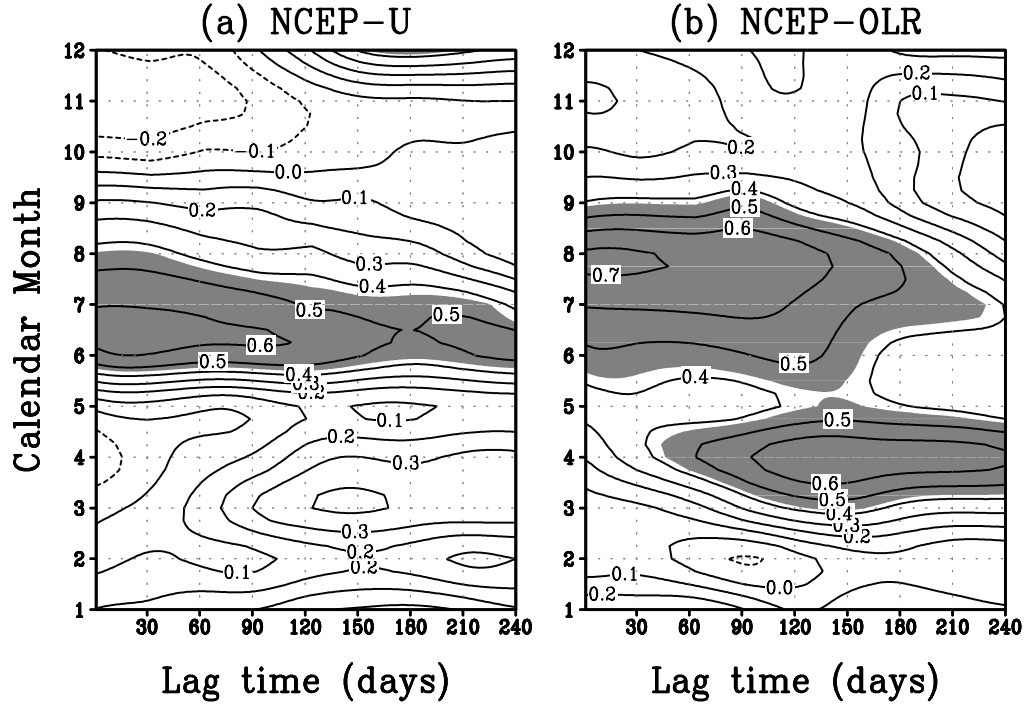


Figure 6: The lagged correlation of MJO indices, as functions of lag time (days) and start month, with Niño3 index. Shaded is the correlation that is statistically significant at a confidence level of 95%.

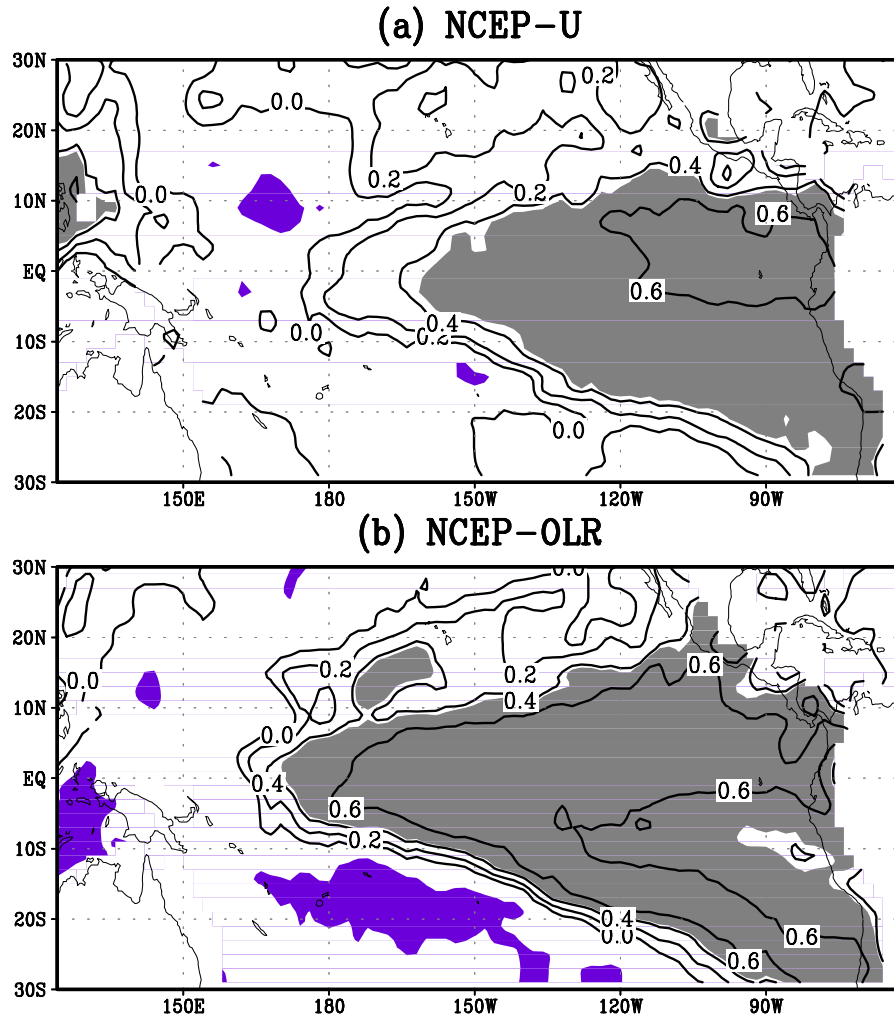


Figure 7: The correlation between MJO indices in July and SSTA in the subsequent October. Shaded is the correlation that is statistically significant at a confidence level of 95%.

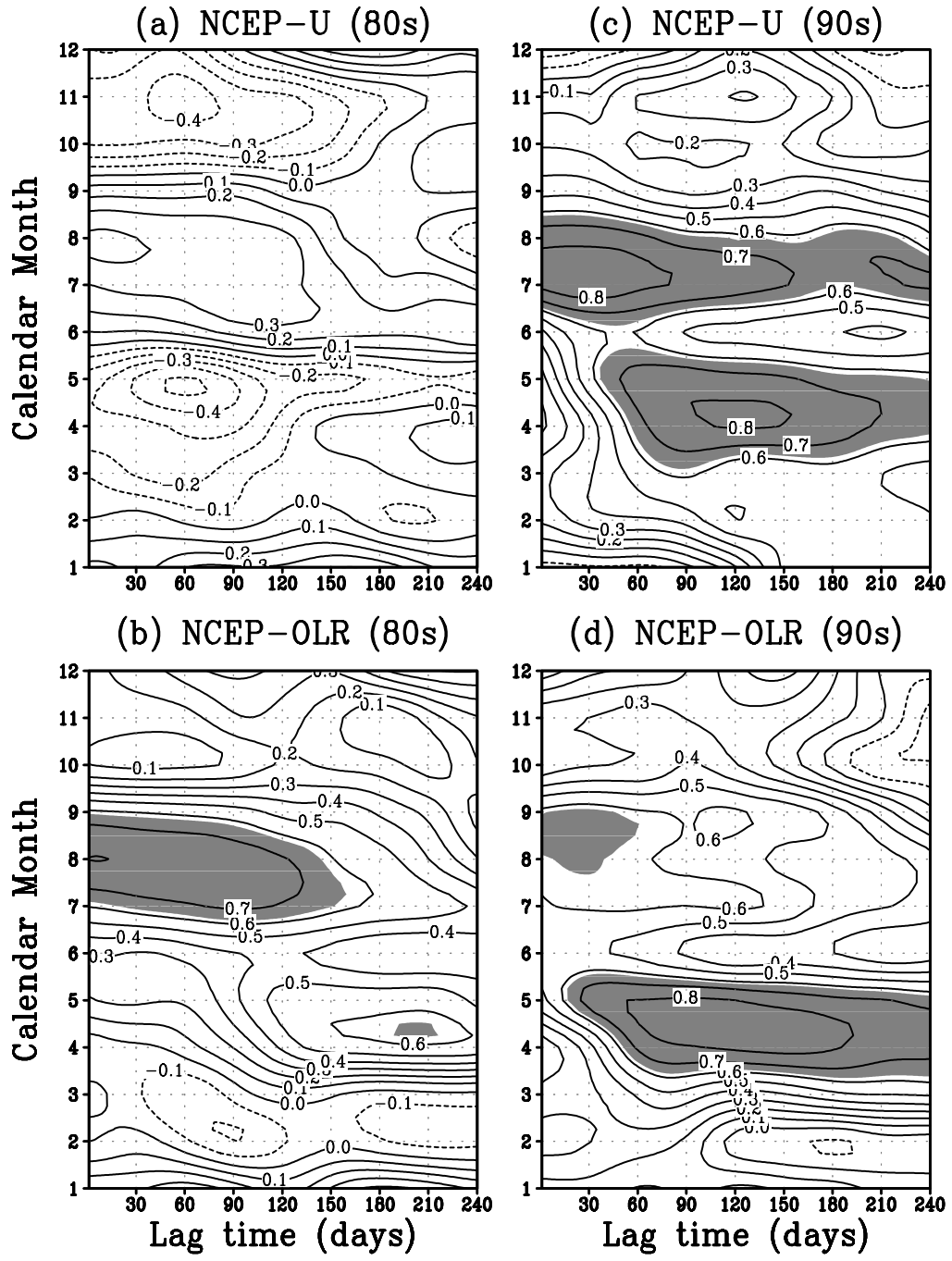


Figure 8: Same as Fig. 6 but for correlations that are computed using the data during the period of 1980s (left panel) and 1990s (right panel) respectively.

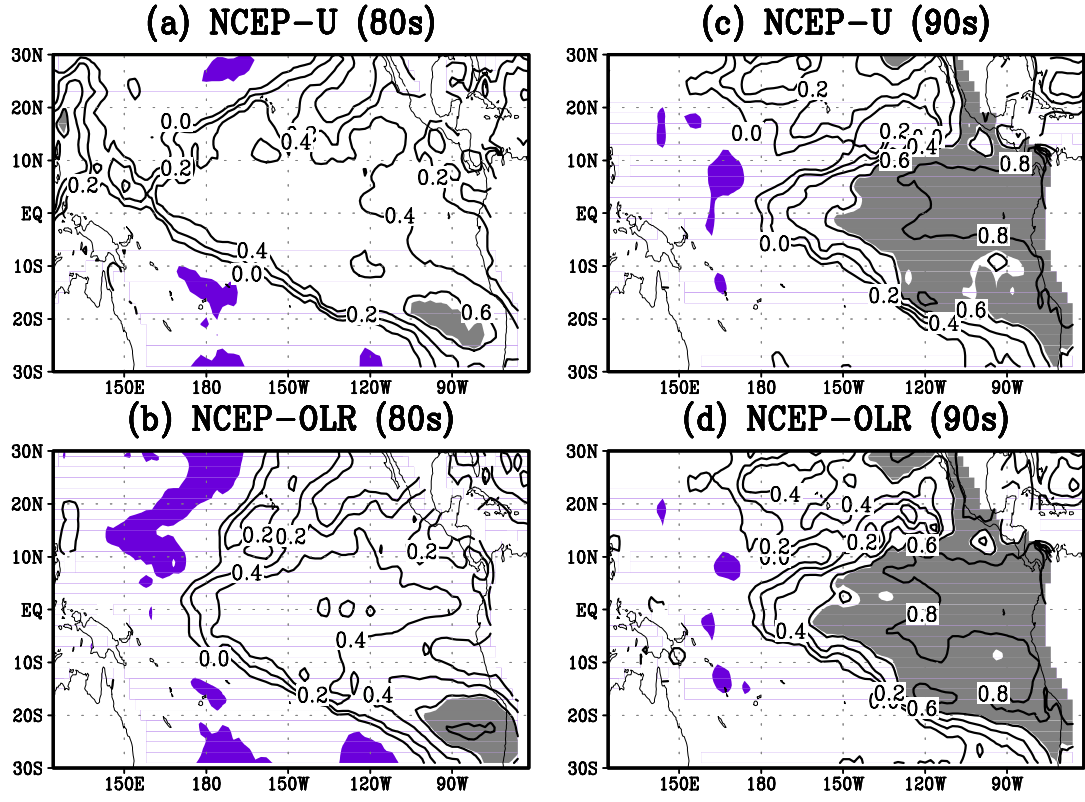


Figure 9: The correlations between the MJO indices in May with SSTA in the subsequent October. Shaded is the statistically significant correlation at the confidence level of 95%. The correlation was respectively computed for the 1980s (a, b) and the 1990s (c,d).

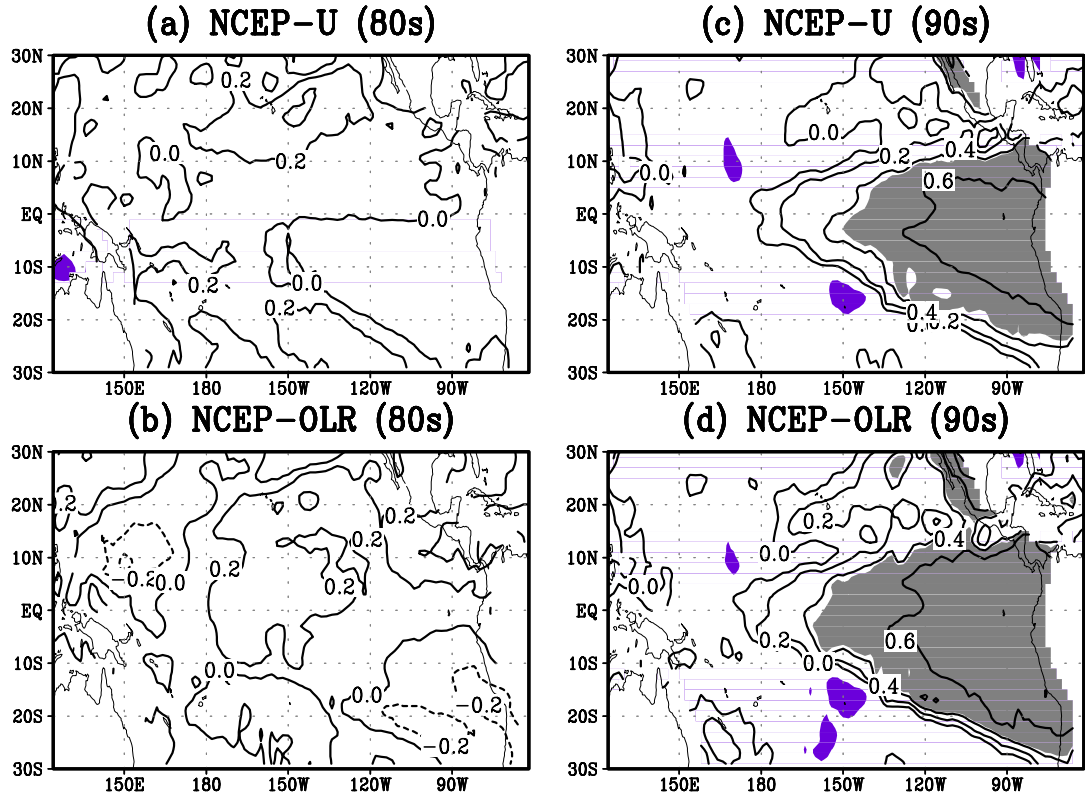


Figure 10: Same as Fig. 9 but for the correlations between MJO in March-May and the tropical SSTA in the subsequent October-December.

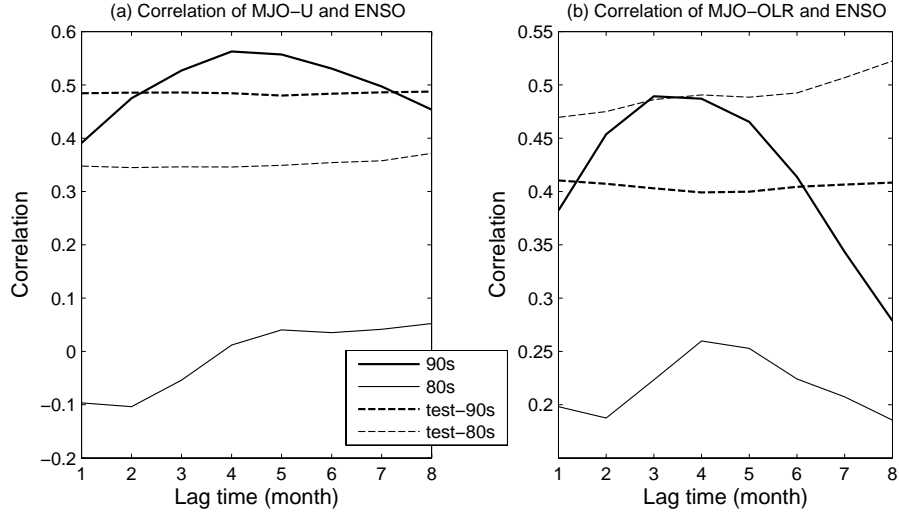


Figure 11: The lagged correlation between MJO and Nino3 SSTA indices, computed for the 1980s and the 1990s respectively. The correlation for the MJO_U index is shown in (a) and for the MJO_{OLR} in (b). The bold-solid line is for the 1990s and thin-solid line for the 1980s. The statistically significant test is shown in dashed line, with bold-dashed line for the 1990s and thin-dashed line for the 1980s.

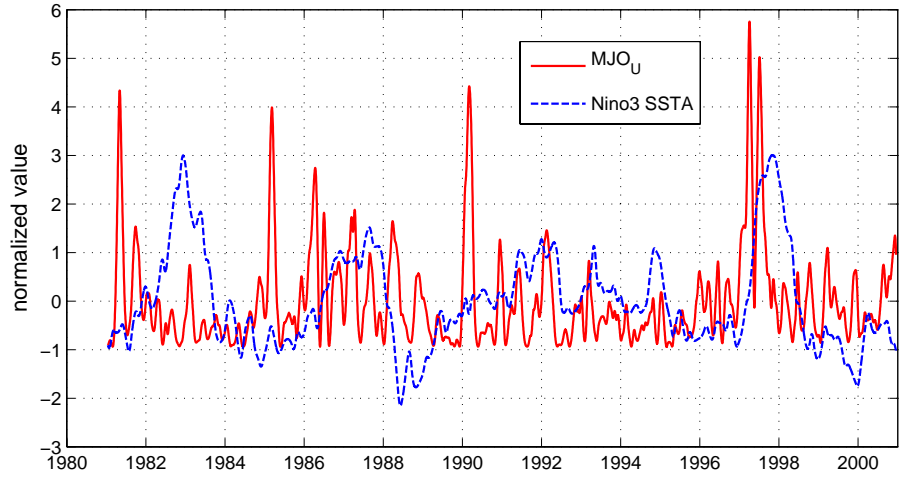


Figure 12: Normalized MJO and Nino3 indices from 1981-2000.

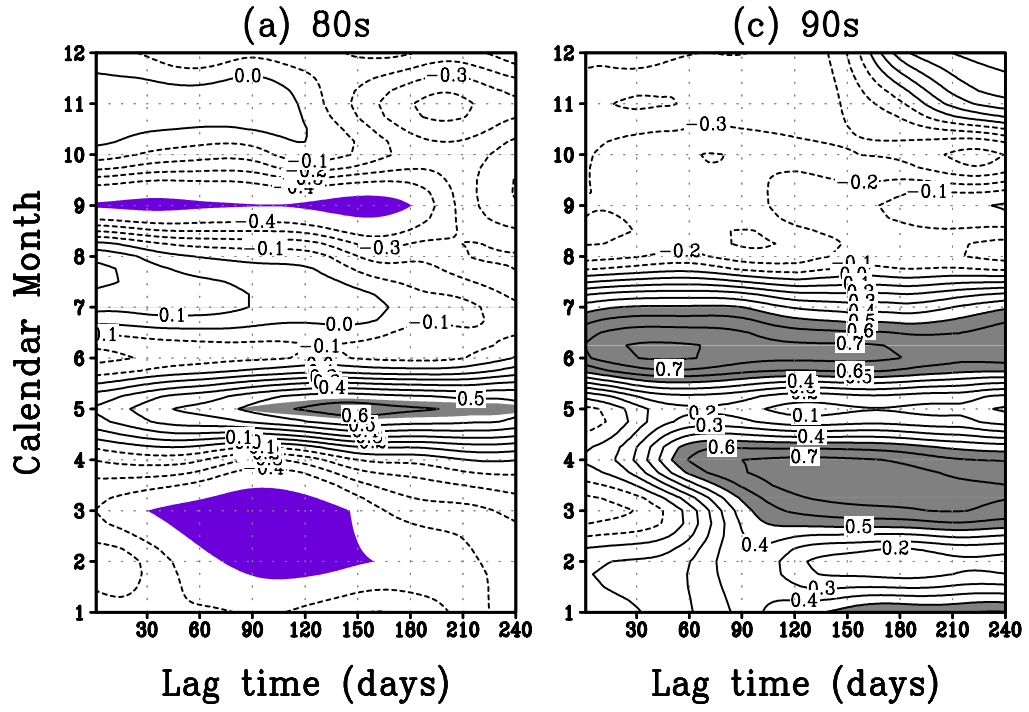


Figure 13: Same as Fig. 8 but for the BMRC MJO index.

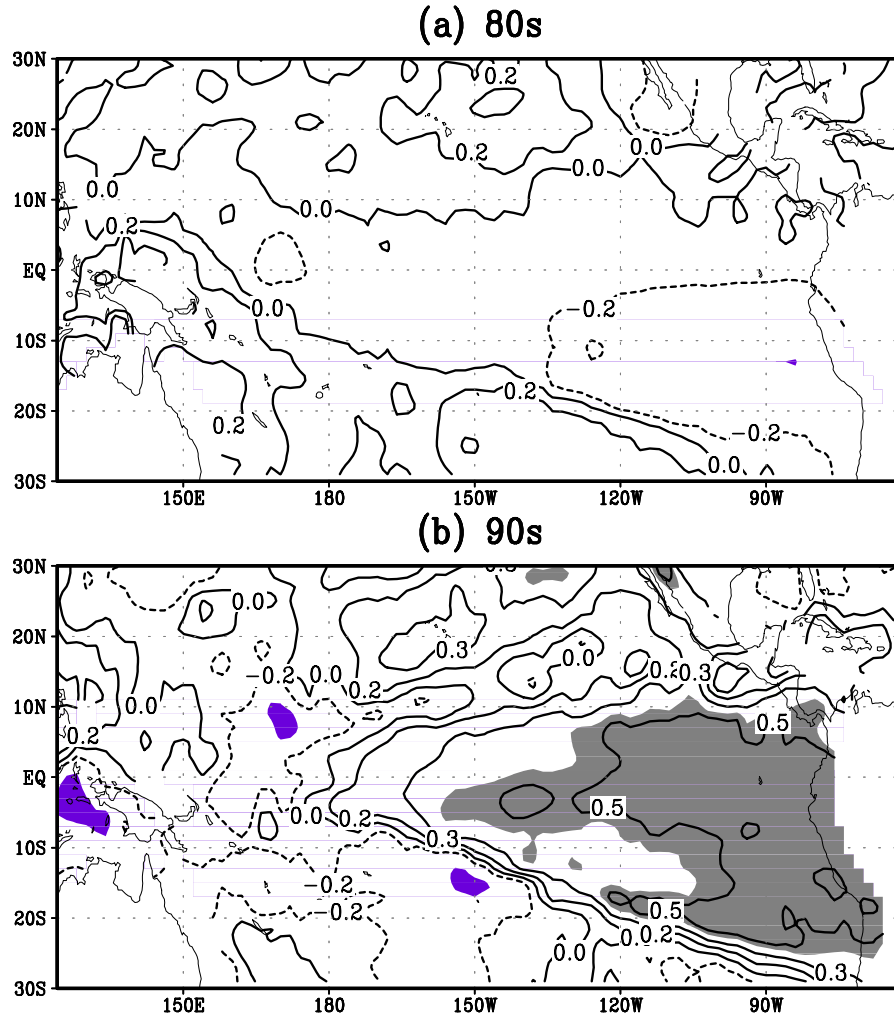


Figure 14: Same as Fig. 10 but for the BMRC MJO index.

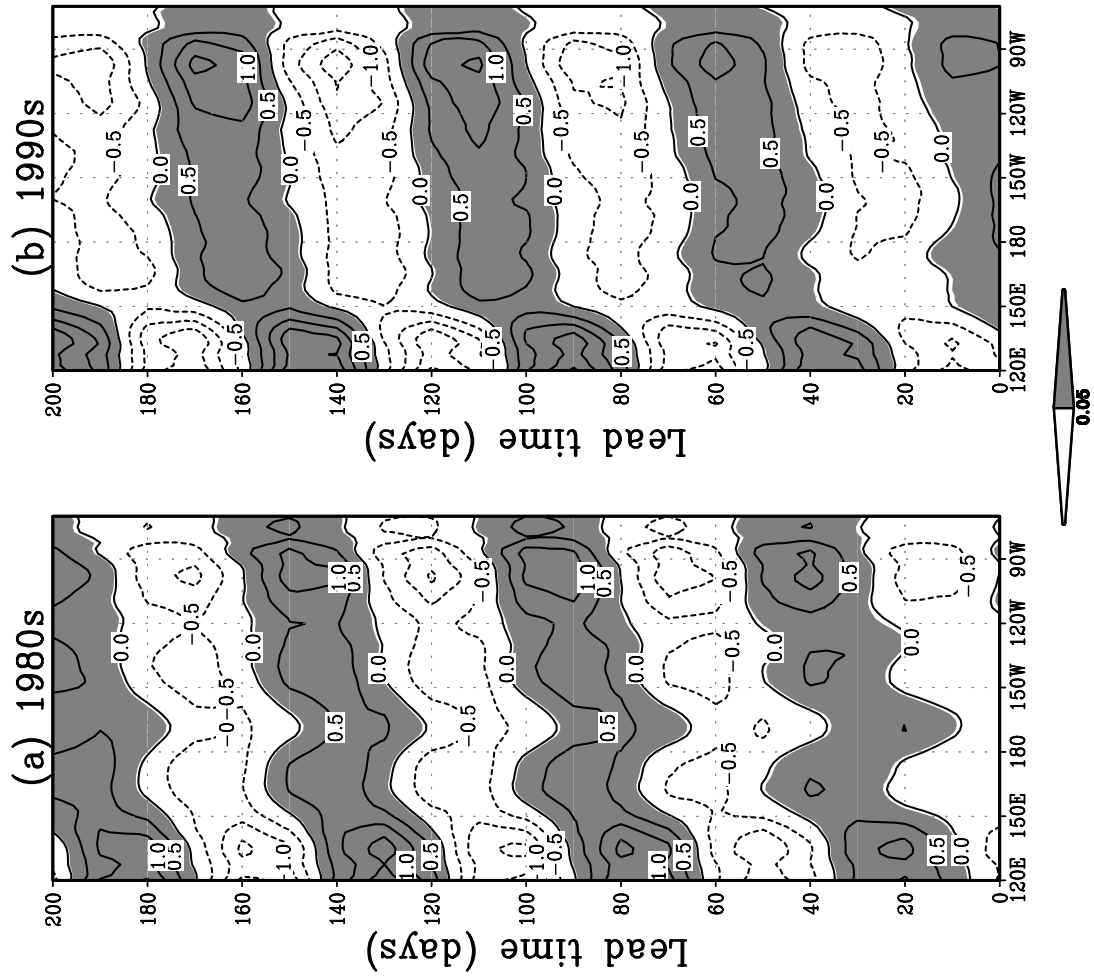


Figure 15: The first EEOF modes of NCEP reanalysis zonal winds for (a) 1980s and (b) 1990s. The unit is $m s^{-1}$ and the contour interval is 0.5.

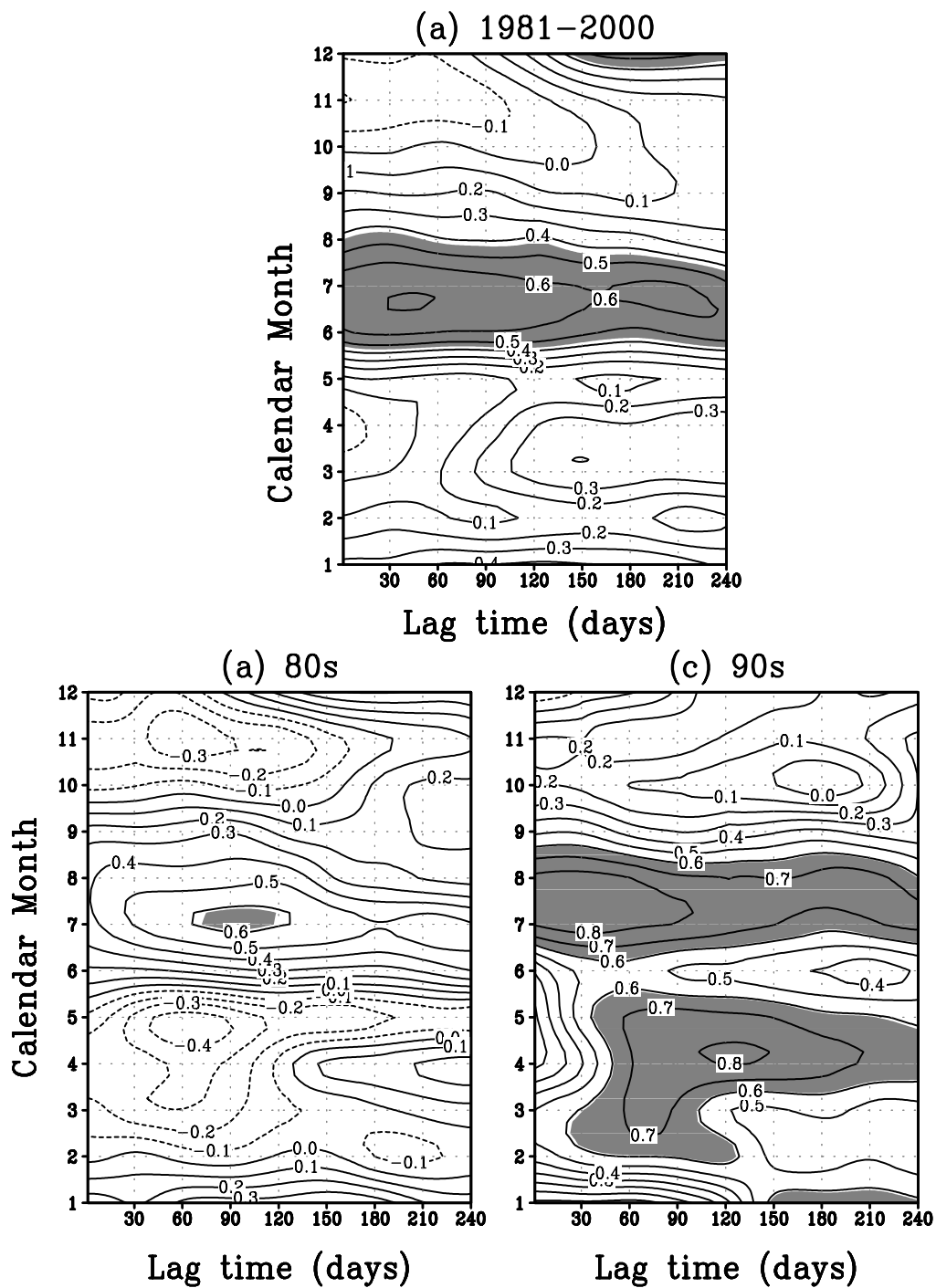


Figure 16: (a) Same as Fig. 6a but for the MJO index that is derived from ECMWF ERA-40 reanalysis zonal winds at the surface. (b) and (c) Same as Fig. 8a and c but for the ERA-40 MJO index.

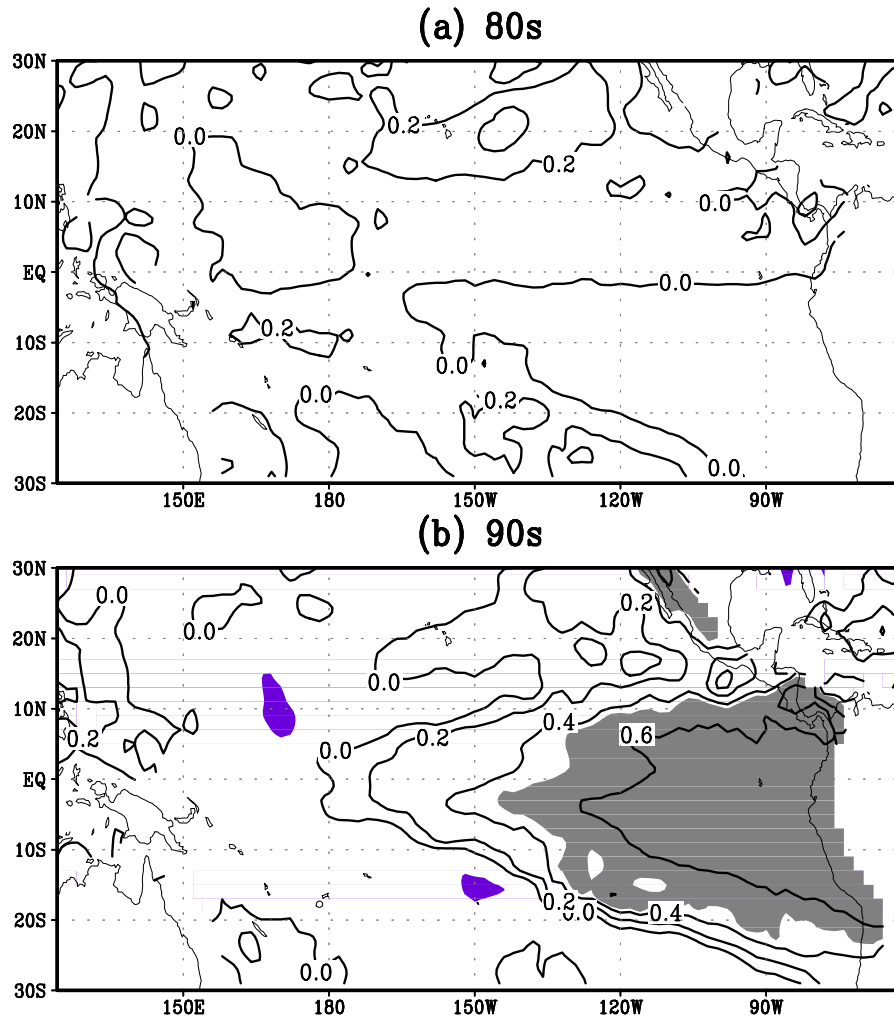


Figure 17: Same as Fig. 10 but for the ERA-40 MJO index.